

# A98-31567

ICAS-98-3,9,4

## IMPROVING THE AERODYNAMIC EFFICIENCY OF A WING BY ACOUSTIC EXCITATION

by

**N.A.Ahmed, R.D.Archer and Heywood M**

**Department of Aerospace Engineering  
School of Mechanical and Manufacturing Engineering  
University of New South Wales  
Sydney NSW 2052, Australia**

### ABSTRACT

*Various active and passive techniques of controlling or suppressing boundary layer have evolved with varying degrees of success since the introduction of the boundary layer concept at the turn of this century. The manipulation of boundary layer flow by acoustic excitation is, however, more of a recent phenomenon and one of the least developed. Most of the work to date has been primarily on two dimensional flat plates or airfoils. In this paper, we look at the performance of a constant NACA0012 symmetric half wing of effective aspect ratio of 4 under external acoustic excitation frequencies ranging from 100 Hz to 3 kHz. Tests were conducted in a open jet low speed wind tunnel when flow has separated on the wing at 16, 17, 18 and 19 degrees of angle of incidence and three different air speeds of 7, 10 and 25m/s respectively. It is found that lift is significantly improved and drag is appreciably reduced thereby improving the lift to drag ratio of the wing to nearly twice its corresponding unexcited value. Such improvement, however, is found to be frequency and Reynolds number dependent.*

### NOMENCLATURE

AR	wing aspect ratio
$C_D$	total wing drag co-efficient
$C_d$	section drag co-efficient of wing
$C_{D0}$	wing parasite drag co-efficient
$C_{Di}$	wing induced drag co-efficient
$C_L$	wing lift co-efficient
$C_l$	section lift co-efficient of wing
Re	Reynolds number based on wing chord and wind tunnel free stream velocity under atmospheric condition
$S_t$	Strouhal number based on wing chord, wind tunnel free stream velocity and acoustic excitation frequency
$\alpha$	angle of attack or incidence
$\delta$	aspect ratio correction factor

### 1.INTRODUCTION

For fixed air properties and free stream, lift can generally be augmented by an increase in either wing area, angle of incidence, camber or artificial circulation. The extent to which these features can be exploited is governed by boundary layer behaviour. Flow separation, which is perhaps, the most important aspect of boundary layer phenomenon but poorly understood, is a major cause of loss in the aerodynamic efficiency of a wing. In subsonic and transonic speeds, where pressure gradients can be particularly severe, a wing can only continue to generate lift successfully if the boundary layer separation is either avoided or closely controlled. Flow separation can, however, take place both in laminar and

21st ICAS Congress  
13-18 September 1998  
Melbourne, Australia

turbulent flows. The situation is further complicated by the fact that instability can easily occur in a laminar flow resulting in its transition to a turbulent flow. Also in many cases, some parts of the flow may remain laminar while other parts become turbulent or have intermittent laminar and turbulent regions. The treatment of flow separation, therefore, poses formidable problems, conceptually, theoretically and experimentally [1,2].

Various techniques such as suction or blowing or circulation control [3-5] have been used to control flow separation with varying degrees of success. These concepts have evolved after Prandtl introduced his boundary layer theory [6] at the turn of this century. The concept of controlling flow separation by acoustic excitation, however, originated much later, possibly with the finding of Sprangler and Wells [7] that sound had a significant effect on boundary layer transition. Since then, various attempts [8-11] have been made to study the mechanism associated with the interaction of external or internal sound energy to control or suppress flow separation. Most of these investigations, however, have been carried out on two dimensional flat plates or airfoils. In this work, we have attempted to look at the effect of external acoustic excitation on a finite aspect ratio wing.

## **2. EXPERIMENT**

### ***A. Experimental setup***

Experiments were performed using the 30 inch (0.76m) diameter open jet, open return, axial flow, low speed wind tunnel of the Aerodynamics Laboratory of the University of New South Wales [ Fig 1 ]. The wind tunnel was powered by a 15 b.h.p compound wound D.C. electric motor driving a fan which had eight blades. The motor is trunion mounted external to, and upstream of the tunnel intake mouth. The motor speed can be varied from 200 to 1700 revolutions per minute to give a velocity range of 0 - 30 m/s. A Betz manometer connected to a Pitot static tube can be used at the test section to obtain airspeed.

The tests were carried out on a wing made of constant NACA0012 cross section of 5.9 inch (150 mm) chord length and 11.8 inch (300 mm)

span. The wing was held on one end to a force balance platform while the other end was left free limiting the flow investigation over a symmetric half wing whose effective aspect ratio was 4.

The balance used is a simple two-axis force balance equipped with two load cells of 25 kg force transducers, one measuring the side force or lift experienced by the model and the other measures the force in the direction of the flow or drag. The outputs from the load cells were amplified and fed into a TDS 360 2-channel digital oscilloscope to facilitate graphical representation of load cell output and averaging of data.

The acoustic signals were generated using a Wharfedale speaker of 15 Ohm impedance and powered by a T0 A PA-C37A amplifier of 120 watt power capacity but rated for a 21 Ohm load. The amplifier had no gain control, so the power had to be varied by varying the input voltage. The signal itself was generated using a Goodwill Instruments GFG-8016D sine wave generator.

A block diagram of the experimental setup and instrumentation is given in Figure 2.

### **B. Test Procedure**

Once the wing was set at a particular angle of incidence, the load cells were allowed to warm up followed by the switching on of the oscilloscope. The amplifier readings were adjusted to zero to an accuracy of  $\pm 250 \mu\text{V}$  reading.

The wind tunnel was then run up to the desired speed and the lift and drag readings were recorded under no-excitation condition. The frequency generator was then set to 100 Hz and the amplifier turned up full. After approximately 10 seconds, the oscilloscope was activated to take readings and an average was obtained after 30 seconds. Once a particular test run was completed, the wind tunnel was switched off and a time was allowed to elapse until the fan stopped completely. The amplifiers were then checked for any drift and zeroed for next test run. Additional no-excitation readings were recorded at 1 kHz and 2 kHz frequencies by

switching off the speakers to observe any drift in amplifier readings. The above procedure was repeated for different angle of incidence settings of the wing and wind tunnel speeds.

Measurements were taken at velocities of 7, 10 and 25 m/s for  $16^\circ$ ,  $17^\circ$ ,  $18^\circ$  and  $19^\circ$  angle of incidence at external excitation frequencies between 100 Hz to 3 kHz in increments of 100 Hz.

### 3. RESULTS AND DISCUSSION

The effect of excitation frequency on lift and drag co-efficients at  $16^\circ$ ,  $17^\circ$ ,  $18^\circ$  and  $19^\circ$  angle of incidence settings of the wing are presented in Figs 3[(a)-(d)] to 5[(a)-(d)] for wind tunnel velocities of 7, 10 and 25 m/s respectively. On the frequency axis, the equivalent  $S_t$  values are also given. Also on these curves two continuous lines are given showing the unexcited values.

Before analysing the data an attempt was made to check the validity of the  $C_L$  and  $C_D$  data obtained. Bearing in mind that we have essentially a symmetric half wing when flow separation has just taken place, these values can only be considered as approximate. From the data on NACA0012 airfoil [12], flow separation occurs at around  $16^\circ$  when the sectional or two dimensional lift co-efficient,  $C_l$  drops dramatically from a value of approximately 1.6. Very approximately then, from standard textbooks on aerodynamics [13], one can use :

$$\begin{aligned} C_L &= 2\pi\alpha - 2C_l(1+\delta)/AR \text{ and} \\ C_{Di} &= C_L^2(1+\delta)/(\pi AR) \text{ so that} \\ C_D &= C_{D0} + C_{Di} \end{aligned}$$

where the values of  $\delta$  lies between 0.05 and 0.25 [14].

$$\begin{aligned} \text{At } \alpha = 16^\circ, \text{ using } AR = 4, C_l = 1.6 : C_L \\ = 0.72 \text{ and } C_{Di} = 0.047 \text{ for } \delta = 0.15 \\ \text{and } C_L = 0.68 \text{ and } C_{Di} = 0.044 \text{ for } \delta = 0.2 \end{aligned}$$

The values obtained at  $\alpha = 16^\circ$  for wind tunnel speed of 7 m/s for the unexcited values of  $C_L$  and  $C_D$  were approximately 0.7 and 0.2. These values were considered to be of the right order of the values obtained.

#### a. Results at 7 m/s [Figures 3(a)-(d)]

These results correspond to a  $Re = 7.2 \times 10^4$ . From Figures 3(a) and 3(b), it can be seen that at  $\alpha = 16^\circ$  and  $17^\circ$ , acoustic excitation improves the  $C_L$  values quite significantly over a wide range of frequencies corresponding to  $S_t$  ranging from 5 to 45. The results generally show 20-30 % increase in lift and 30-35 % decrease in drag resulting nearly in doubling of the lift to drag ratio over their unexcited values. At  $\alpha = 18^\circ$  and  $19^\circ$  [Figures 3(c) and 3(d) respectively], the results are significantly different. The improvements are limited to a lower range of frequencies below  $S_t$  values of 25. At  $\alpha = 18^\circ$  [Figure 3(c)], the improvements in lift and drag coefficients are still significant with increases of upto 35% and 25 % respectively over their unexcited values. At  $\alpha = 19^\circ$  [Figure 3(d)], the larger gains produced at lower angle of incidence are absent with improvements of only 10-20 % in lift and 10% in drag respectively.

#### b. Results at 10 m/s [Figures 4(a)-(d)]

These results correspond to a  $Re = 10.3 \times 10^4$ . At 10 m/s, there is an obvious shift to higher frequencies compared to that observed at 7 m/s, above 1500 Hz ( $S_t > 22.5$ ) to around 2600 Hz ( $S_t = 40$ ), when lift and drag values are improved. The improvements are of the order of 30-40 % increase in lift and up to 30 % decrease in drag resulting in nearly doubling of the lift to drag ratio. At  $\alpha = 19^\circ$  [Figure 4(d)], the effects show considerable abatement with improvements of only 10 % in lift and negligible decrease in drag over their unexcited values.

#### c. Results at 25 m/s [Figures 5(a)-(d)]

These results correspond to  $Re = 25.7 \times 10^4$ . At 25 m/s, there is again further shift to higher frequencies compared to those observed for 7 m/s and 10 m/s respectively, above 1700 Hz ( $S_t > 10$ ) to around 2600 Hz ( $S_t = 15$ ). Significant performance in lift and drag values are evident only at lower angle of incidence of  $16^\circ$  [Figure 5(a)].

#### 4. CONCLUSIONS

The results of the experiments conducted at the lower velocities of 7m/s and 10m/s clearly demonstrate that the performance of a finite aspect ratio wing can be considerably improved through the use of acoustic excitation particularly at  $\alpha = 16^\circ$ ,  $17^\circ$  and  $18^\circ$  which are about  $3^\circ$  higher than the angle at which flow separation on NACA0012 airfoil section occurs. The excitation effects are more pronounced at higher frequencies when the Reynolds number of the flow is increased. Although this trend was clearly evident at 25 m/s, when the overall improvement in aerodynamic efficiency of the wing was not quite as significant when compared to lower velocity cases of 7 m/s and 10 m/s. This may be because the effective Strouhal no range [ $St = 10 - 15$ ] was much lower than for 10 m/s [ $St = 22.5 - 40$ ] or 7 m/s [ $St = 5 - 45$ ]. On two dimensional airfoil experiments [15], improvements have been observed at higher Re and higher angle of attack when sound pressure level is increased. All our experiments were, however, conducted at the highest sound pressure level available and further increases were not possible due to equipment performance limitation.

#### 5. REFERENCES

1. Smith, A.M.O., 'Wing design and analysis- your job', in Numerical and Physical aspects of aerodynamic flows II, ed. T.Cebeci, pp41-59, Springer Verlag, 1984
2. Fu, T., Shekarri, A., Katz, J., and Huang, T., 'The structure in the lee side of a 6:1 inclined prolate spheroid', JFM, 269, pp79-106, 1994
3. Pfenninger W and Reed V D, 'Laminar flow: Research and experiments', Astro Aero, 4(7), pp 44-50, 1966
4. Holmes B J, Obara C J and Yip LP, 'Natural laminar flow experiments on modern airplane surfaces', NASA TP-2256, 1984
5. Englar RJ and Huson GG, 'Development of advanced circulation control wing high lift airfoils', J of Aircraft 12 (7), pp 476-483, 1984
6. Schlichting H, 'Boundary layer theory', McGraw Hill Book Company, pp378-382, 7th edition reissued in 1987
7. Sprangler, JG and Wells CS, 'Effects of upstream disturbances on boundary layer transition', AIAA Journal (Technical note), vol 6, Jan-Jun, 1968
8. Ahuja KK and Burrin RH, 'Control of flow separation by sound', AIAA Paper No 84-2298, Oct, 1984
9. Bar-Sever A, 'Separation control on an airfoil by periodic forcing', AIAA Journal (Technical note) vol 27, June, 1989
10. Zaman KBMQ, 'Effect of acoustic excitation on stalled flows over an airfoil', AIAA Journal, vol 30, June, 1992
11. Chang RC, Hsiao FB and Shyu RN, 'Forcing level effects of internal acoustic excitation on the improvement of airfoil performance', J of Aircraft, vol 29, Sept-Oct, 1992
12. Abbot IH and von Doenhoff AE, 'Theory of wing sections', Dover publications, p462, 1955
13. Anderson JD Jr, 'Fundamentals of aerodynamics', McGraw Hill Inc, 2nd edition, pp342, 1991
14. Glauert H, 'The elements of Aerofoil and screw theory', Cambridge University Press, London, 1926
15. Ahuja KK, Whipkey RR and Jones GS, 'Control of turbulent boundary layer flows by sound', AIAA Paper No 83-0726, April, 1983

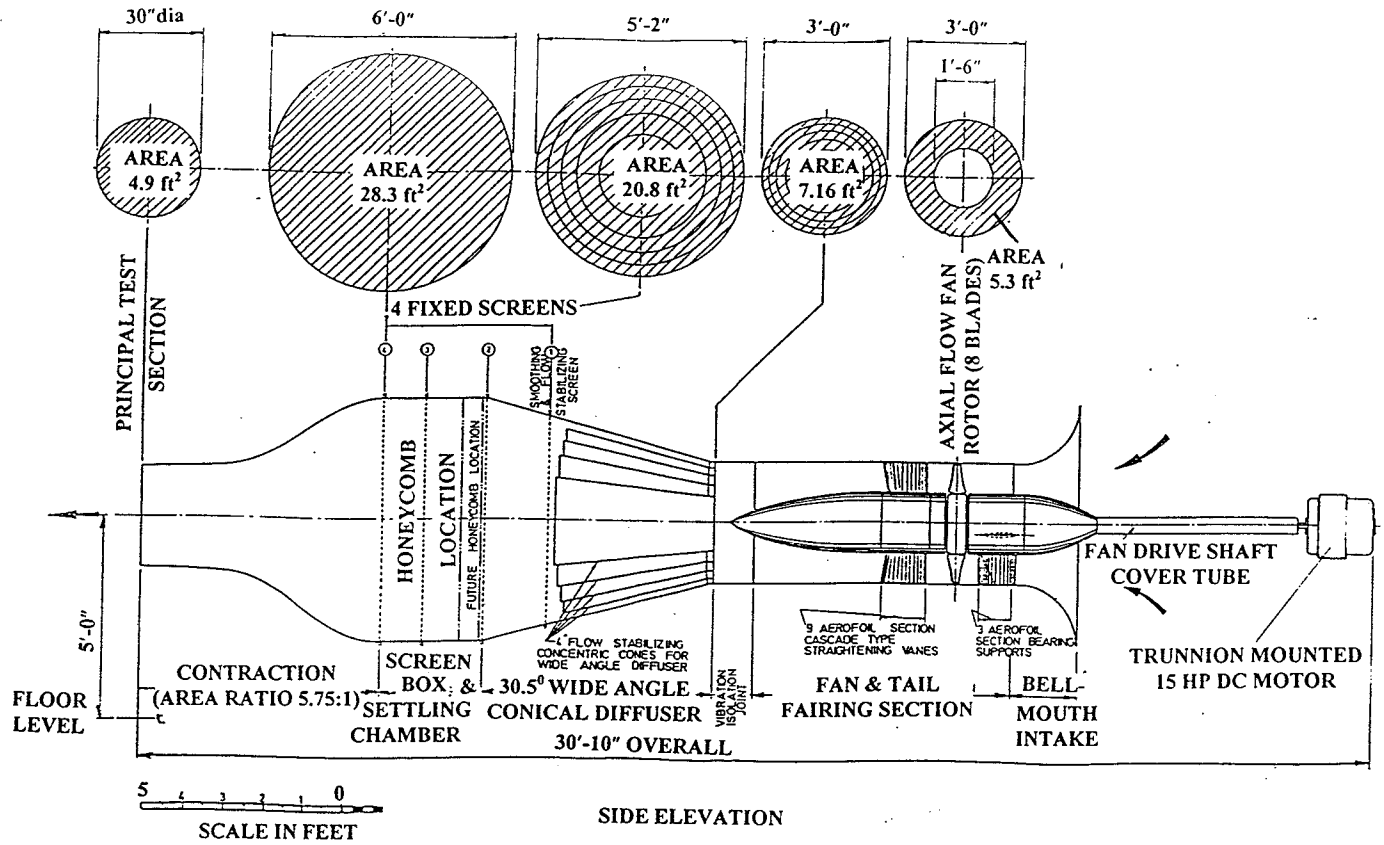


Figure 1 : A diagram of the 30 inch open jet wind tunnel

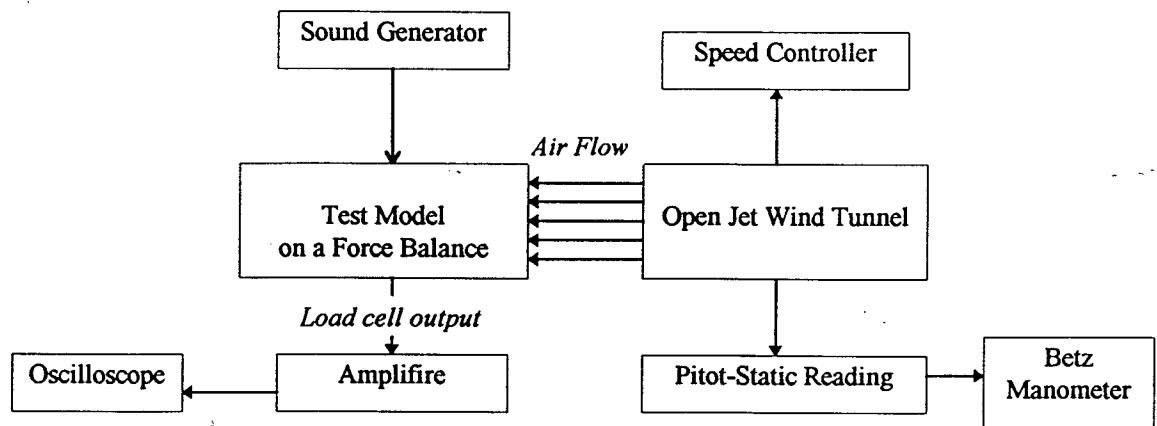


Figure 2: Block diagram of experimental set up and instrumentation.

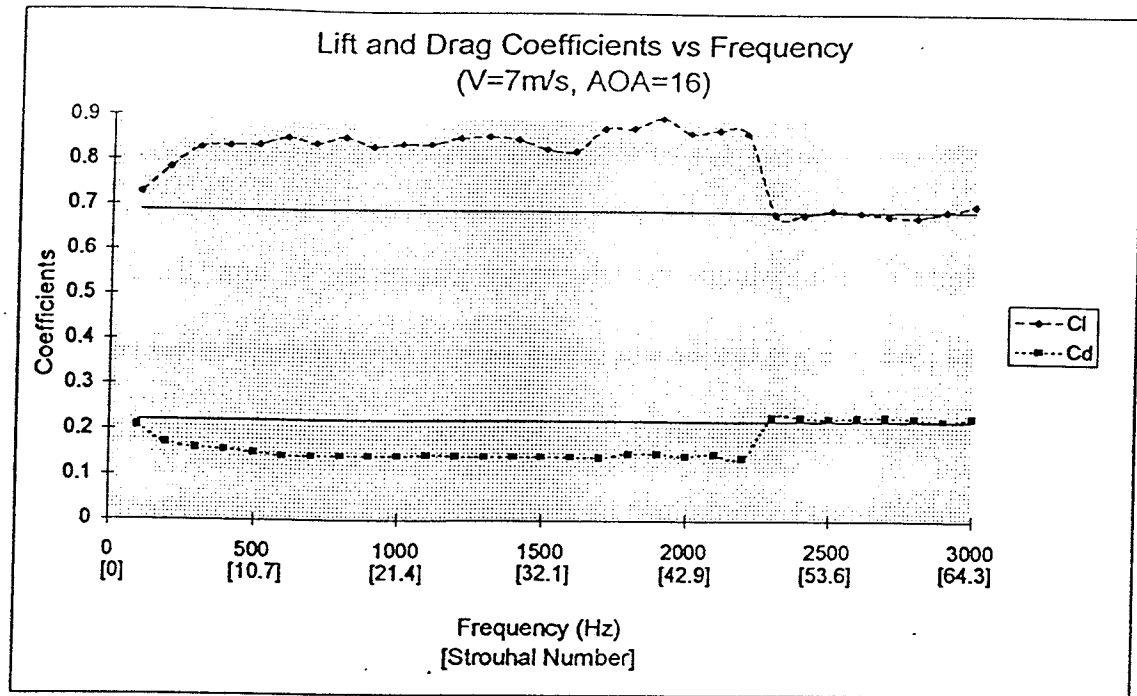


Figure 3(a)

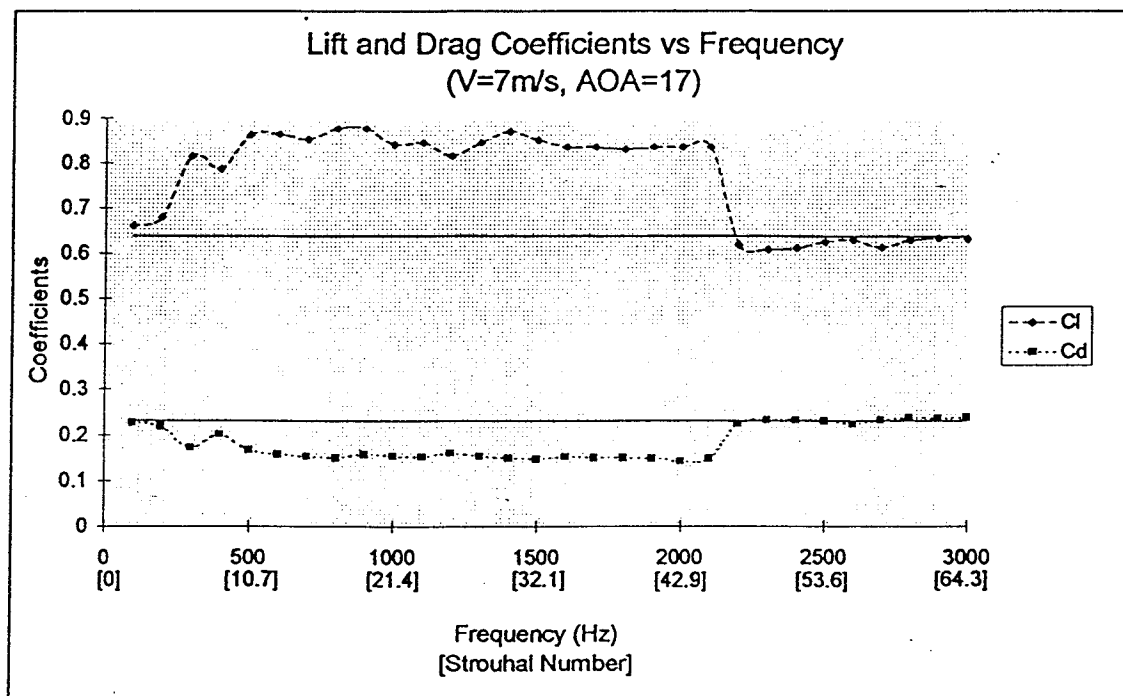


Figure 3(b)

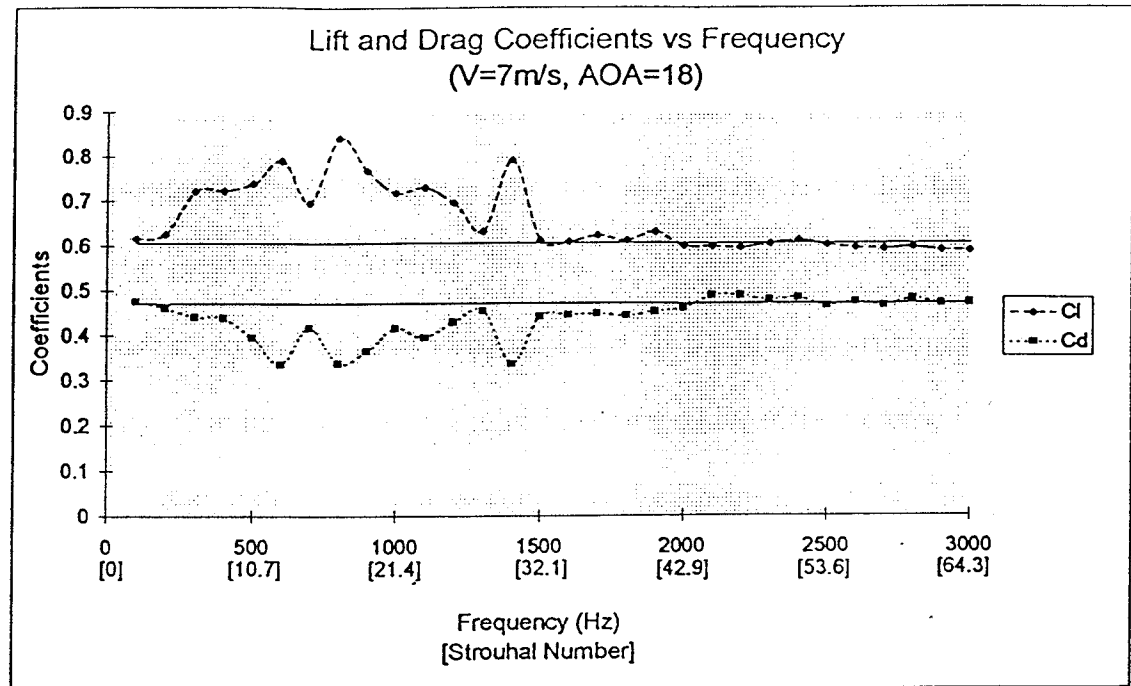


Figure 3(c)

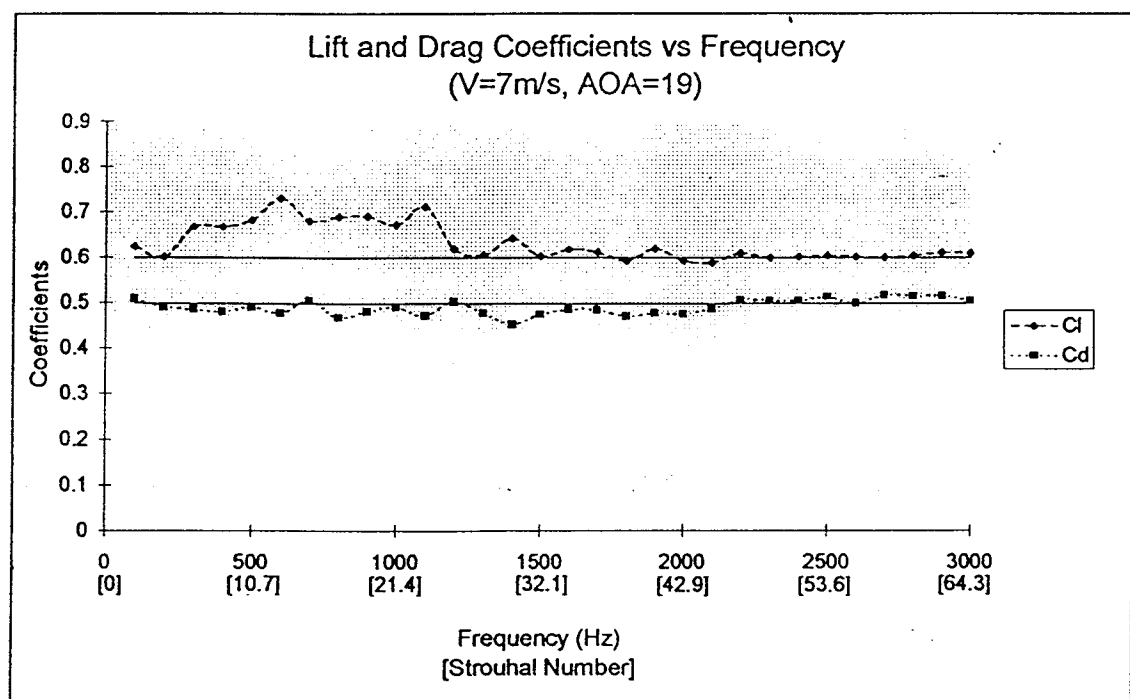


Figure 3(d)

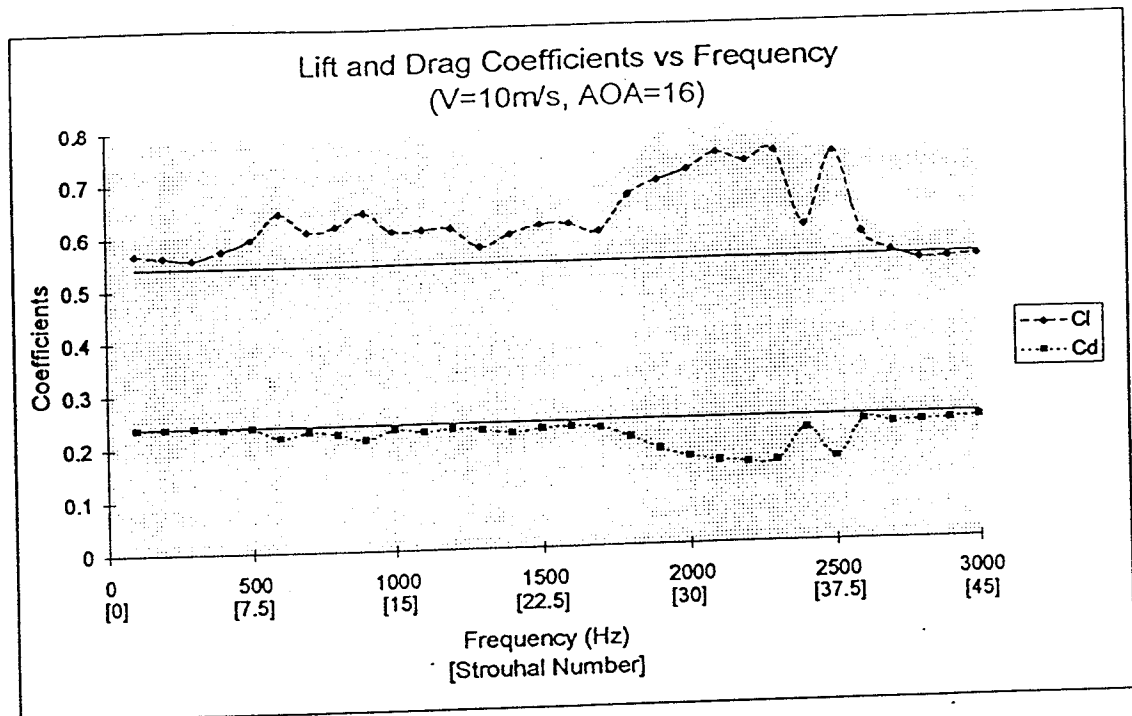


Figure 4(a)

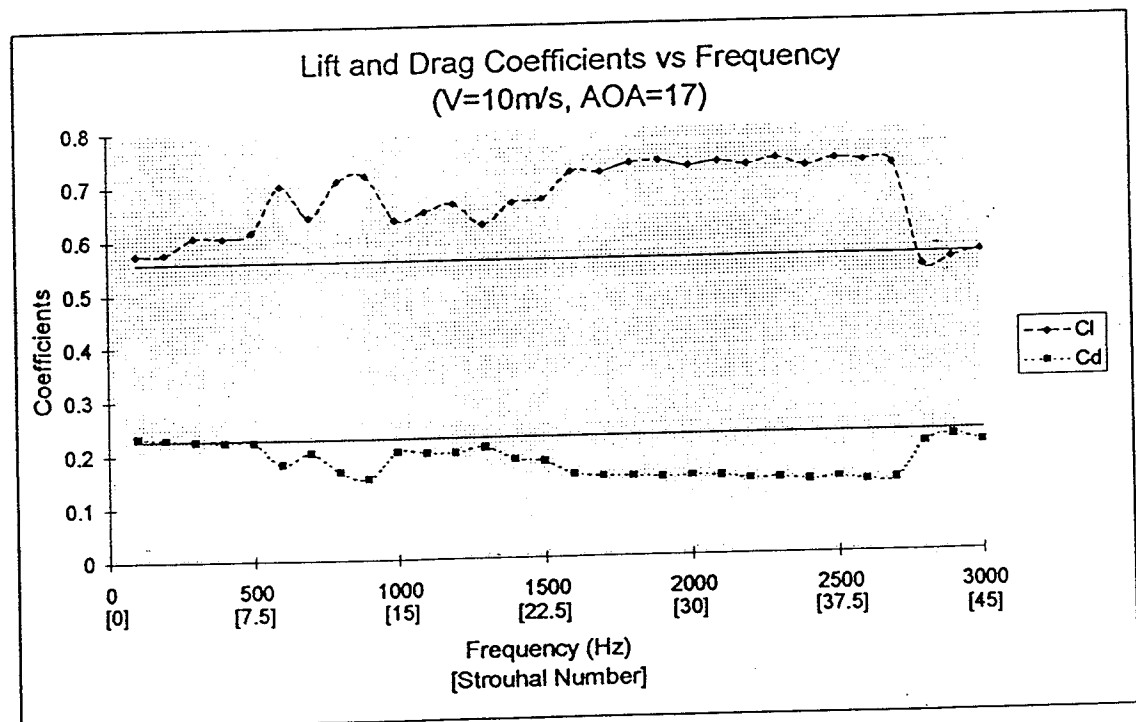


Figure 4(b)



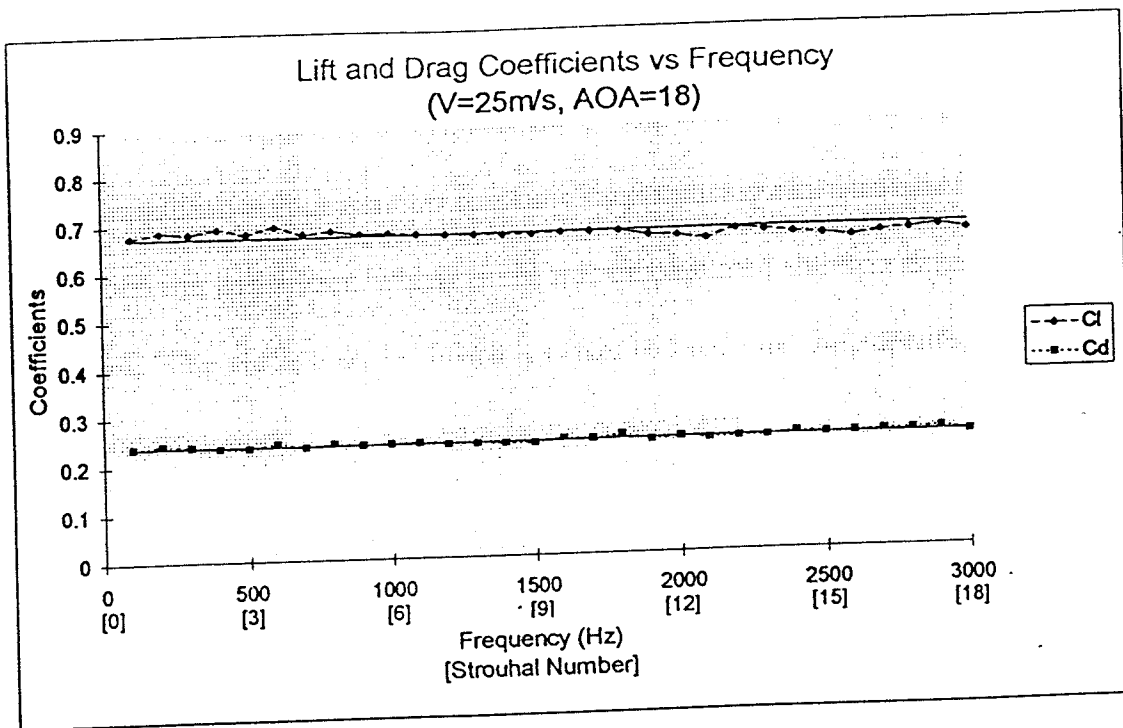


Figure 4(c)

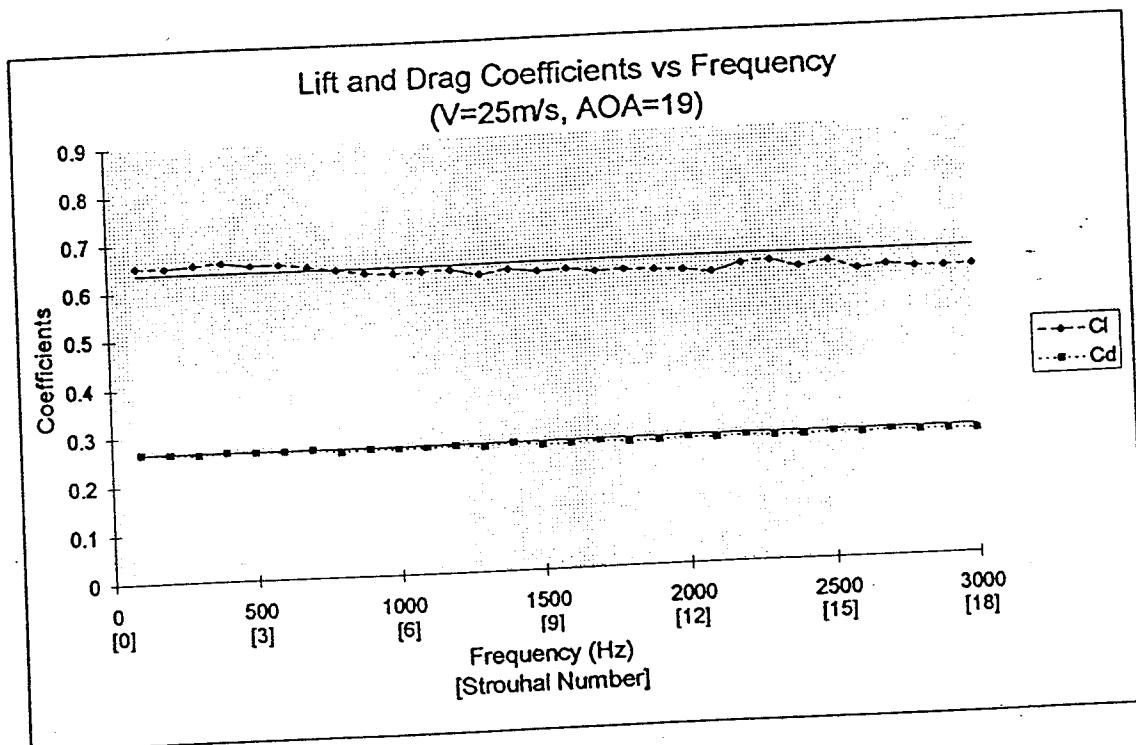


Figure 4(d)

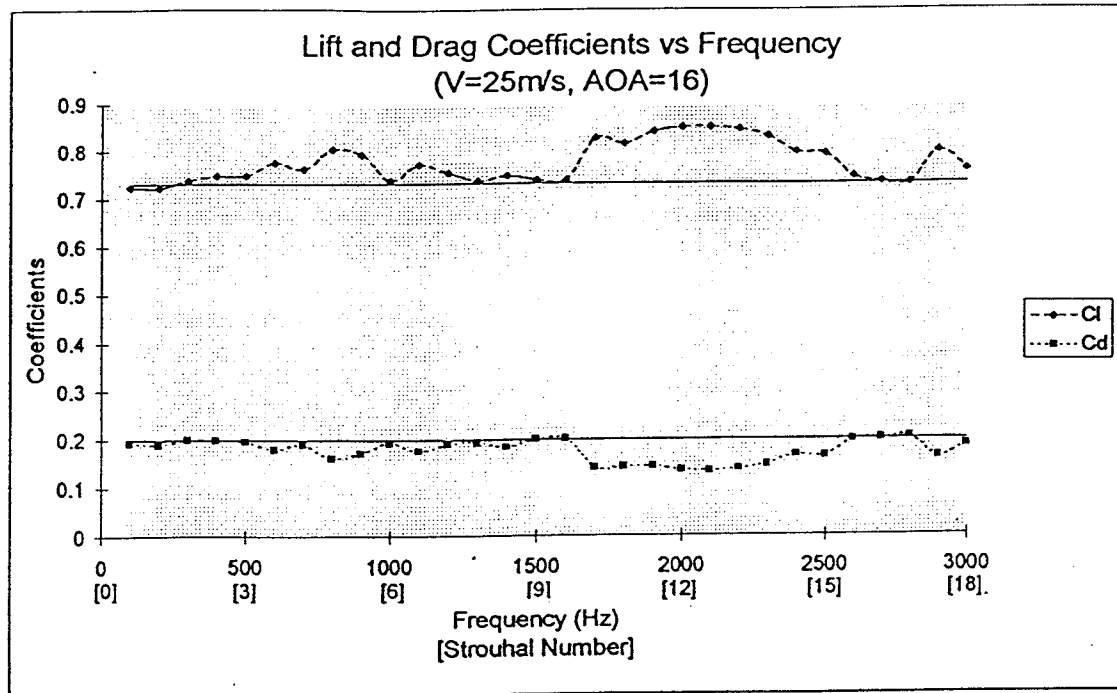


Figure 5(a)

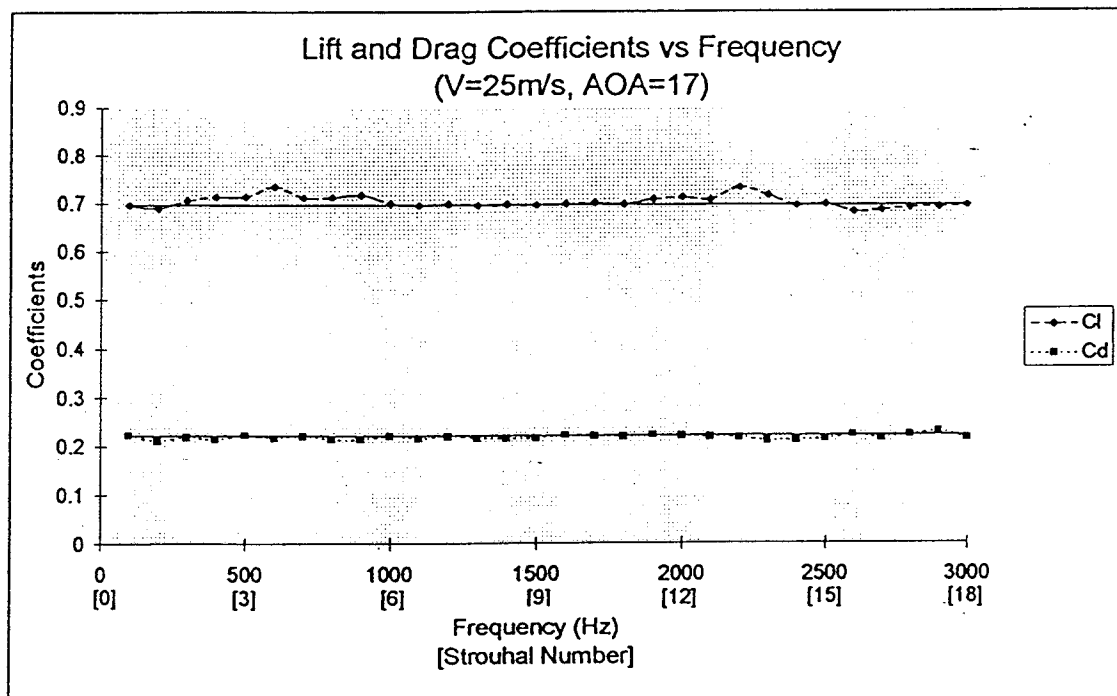


Figure 5(b)

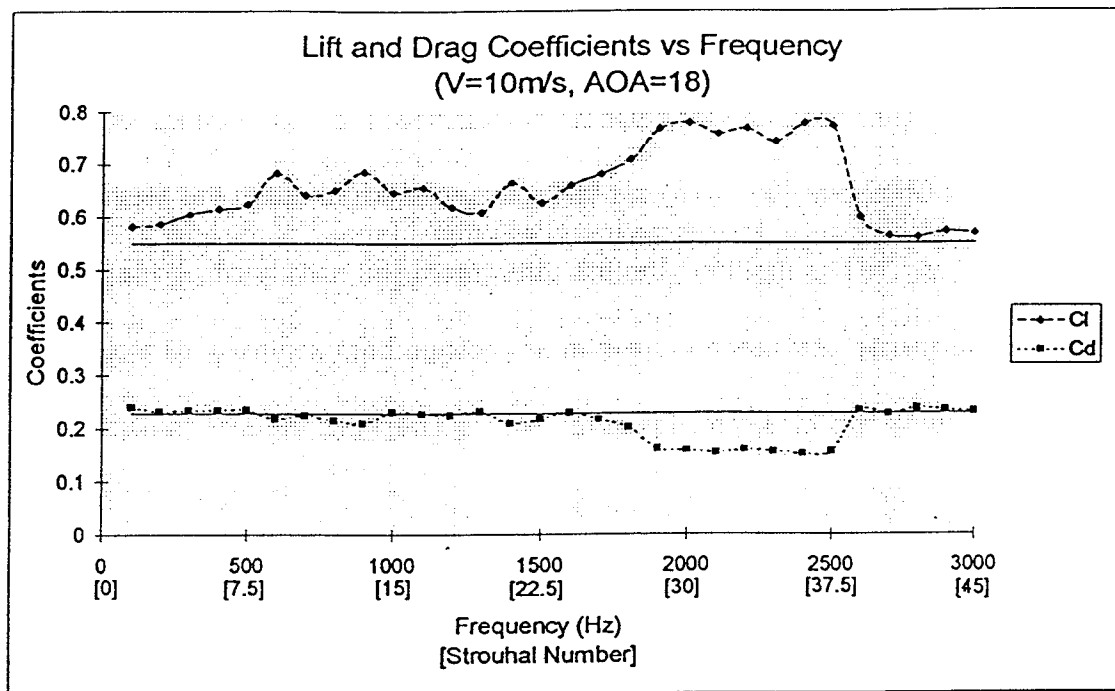


Figure 5(c)

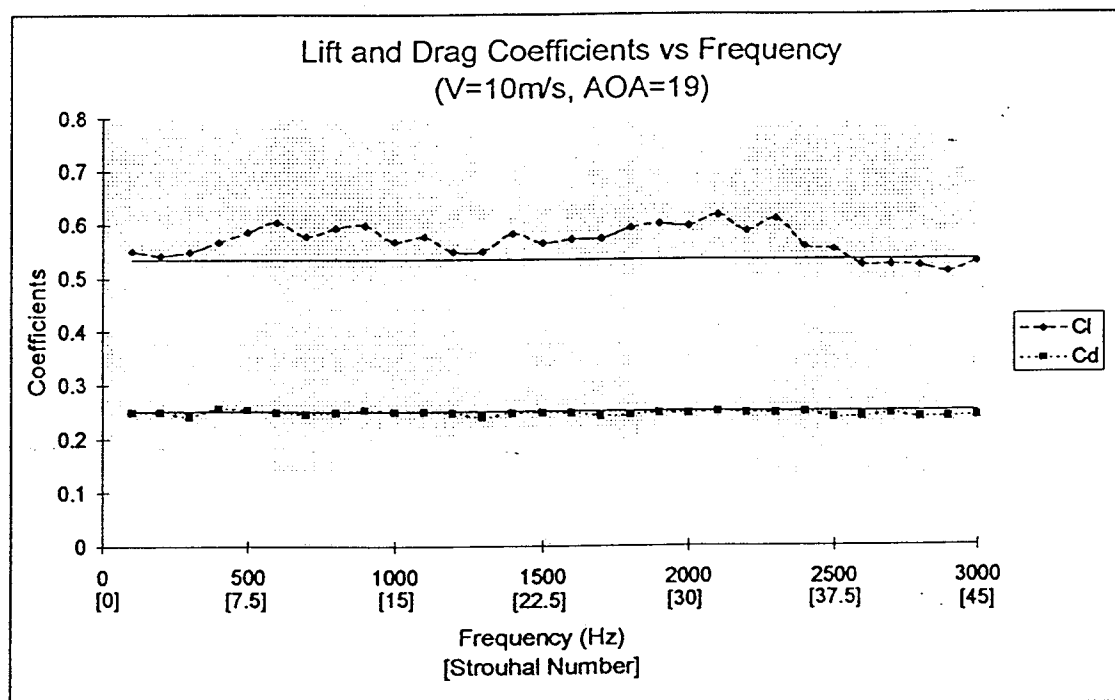


Figure 5(d)